Electronic Supplementary Material (ESI) for Inorganic Chemistry Frontiers.

Supporting Information

Cr^{3+}-doped double perovskite antimonates, efficient and tunable phosphors from NIR-I to NIR-II

Meng Zhao, Shengqiang Liu, Hao Cai, Fangyi Zhao, Zhen Song*, Quanlin Liu*

The Beijing Municipal Key Laboratory of New Energy Materials and Technologies, School of Materials Sciences and Engineering, University of Science and Technology Beijing, Beijing 100083, China.

* Corresponding author: E-mail: qlliu@ustb.edu.cn (Quanlin Liu)

* Corresponding author: E-mail: zsong@ustb.edu.cn. (Zhen Song)

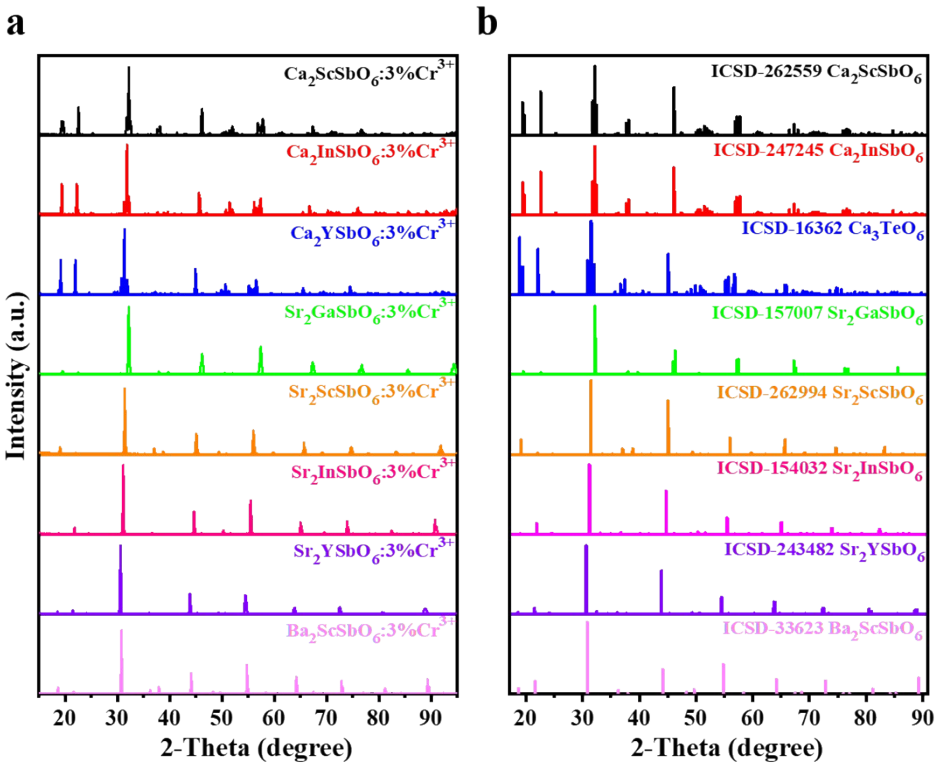

Figure S1 XRD patterns of (a) $A_2MSbO_6:Cr^{3+}$ (A = Ca, Sr, and Ba; M = Ga, Sc, In, and Y) and (b) standard PDF cards. Owing to the absence of structural information on Ca_2YSbO_6, we used the crystallographic data of Ca_3TeO_6 (ICSD-16362) as the initial structural model.[S1]

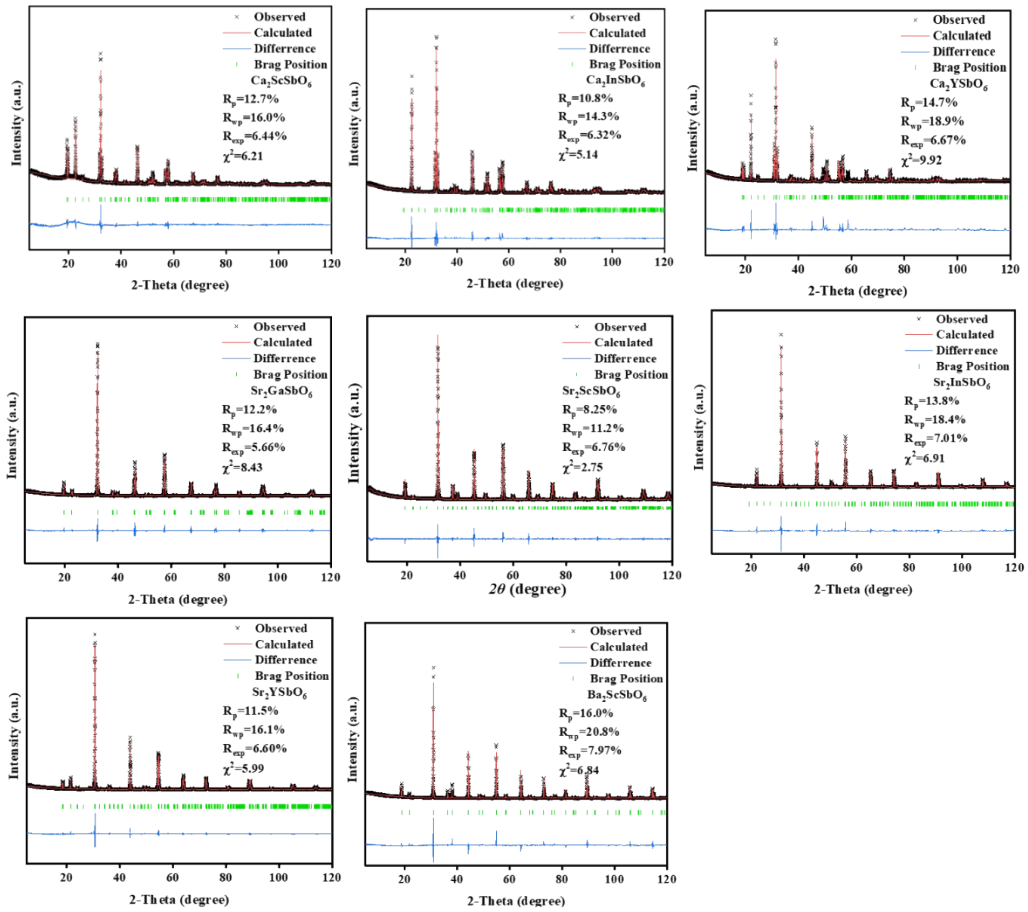

Figure S2 Rietveld refinement of $A_2MSbO_6:Cr^{3+}$ including observed (black cross), calculated (red line), Bragg reflection peaks (green bar) and difference (blue line).

Table S1. Main parameters of processing and refinement of A_2MSbO_6 samples.

Compound	Ca_2ScSbO_6	Ca_2InSbO_6	Ca_2YSbO_6	Sr_2GaSbO_6	Sr_2ScSbO_6	Sr_2InSbO_6	Sr_2YSbO_6	Ba_2ScSbO_6
Space Group	*P 1 21/n 1*	*P 1 21/n 1*	*P 1 21/n 1*	*I 4/m*	*P 1 21/n 1*	*P 1 21/n 1*	*P 1 21/n 1*	*F m -3 m*
Symmetry	Monoclinic	Monoclinic	Monoclinic	Tetragonal	Monoclinic	Monoclinic	Monoclinic	Cubic
Z	1	1	1	1	1	1	1	2
a(Å)	5.49(7)	5.51(9)	5.58(8)	5.54(5)	5.68(5)	5.72(2)	5.80(8)	8.19(7)
b(Å)	5.62(2)	5.68(1)	5.79(0)	5.54(5)	5.67(1)	5.71(9)	5.83(3)	8.19(7)
c(Å)	7.84(8)	7.89(1)	8.03(9)	7.88(7)	8.01(3)	8.08(7)	8.22(8)	8.19(7)
$\alpha = \gamma$(°)	90.00	90.00	90.00	90.00	90.00	90.00	90.00	90.00
β(°)	90.01	89.92	90.06	90.00	90.05	90.04	89.83	90.00
V(Å^3)	243.46	248.77	258.89	242.36	259.35	265.87	278.82	275.98

Calculation of optical band gap

The Tauc relation can be used to calculate the optical band gap Eg, as shown in Equation (S1) [S2]:

$$\left[F\left(R_{\infty}\right)h\upsilon\right]^{n}=A\left(h\upsilon-E_{g}\right) \quad \text{(S1)}$$

where hv represents the energy of interaction between lattice vibration and electronic transition; A is a constant; for n = 2, the calculated result represents the direct transition of A_2MSbO_6; $F(R_\infty)$ is defined using the Kubelka-Munk function, as shown in Equation (S2):

$$F\left(R_{\infty}\right)=\frac{\left(1-R\right)^{2}}{2R} \quad \text{(S2)}$$

where R is the reflectance coefficient. Fig. S3 shows that the calculated optical band gap for different A_2MSbO_6 ranges from 3.3 to 4.2 eV.

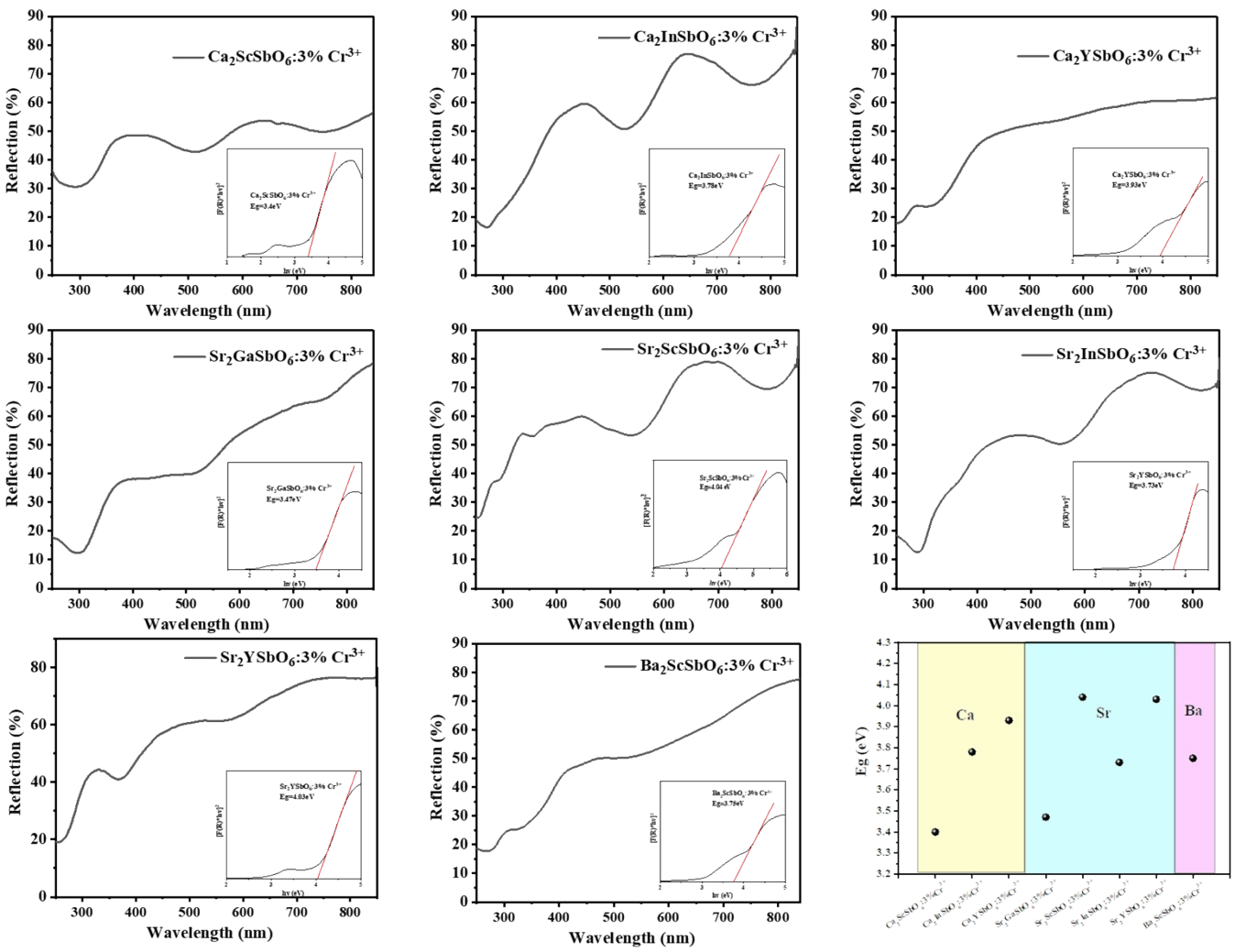

Figure S3. UV diffuse reflection spectra of A_2MSbO_6:3%Cr^{3+}. The inset shows the DR spectrum of the A_2MSbO_6:3%Cr^{3+} host with $[F(R)*hv]^2$ as a function of photon energy, for determining the band gap energy.

Calculation of crystal field parameters

The local crystal field parameter 10Dq/B can be obtained by equations (S3-5).[S3-S5]

$$10Dq = E\left({}^4T_2\right) = E\left({}^4A_2 \rightarrow {}^4T_2\right) - \Delta S/2 \tag{S3}$$

$$\frac{B}{Dq} = \frac{\left(\frac{\Delta E_{4T}}{Dq}\right)^2 - 10\left(\frac{\Delta E_{4T}}{Dq}\right)}{15\left(\frac{\Delta E_{4T}}{Dq} - 8\right)} \tag{S4}$$

$$\Delta E_{4T} = E\left({}^4T_1\right) - E\left({}^4T_2\right) \tag{S5}$$

where *Dq* is the crystal field strength parameter, *B* is the Racah parameter. Stokes shift (*⊿S*) is derived by the energy difference between the $^4A_2(^4F) \rightarrow {}^4T_2(^4F)$ excitation peak and the $^4T_2(^4F) \rightarrow {}^4A_2(^4F)$ emission peak.

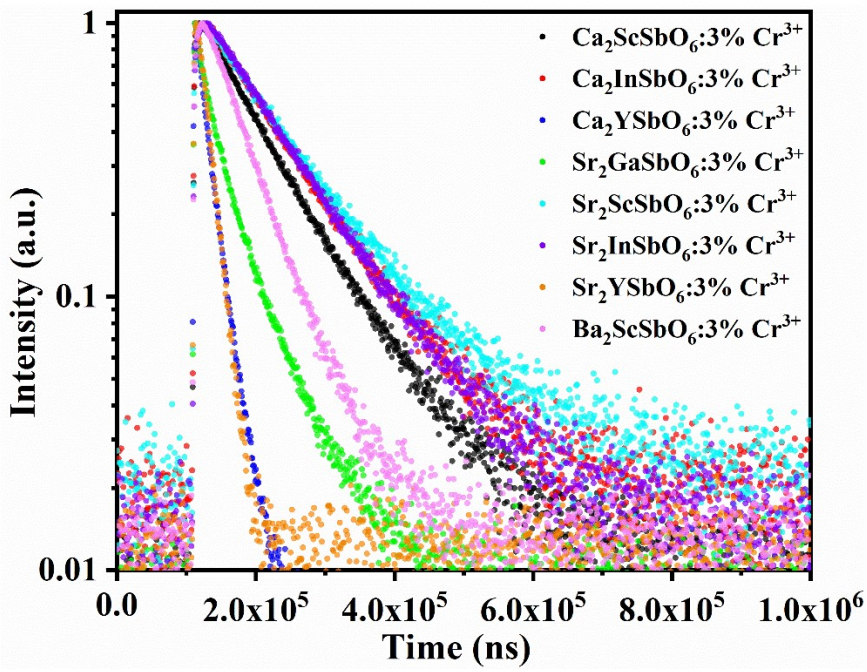

Figure S4. Luminescence decay curves of A_2MSbO_6:3%Cr^{3+}.

Table S2 Decay lifetimes of several Cr^{3+} doped near infrared phosphors.

NIR Phosphor	Decay lifetime (μs)	Wavelength (nm)	Reference
$Ca_2ScSbO_6:Cr^{3+}$	98.9	850	This work
$Ca_2InSbO_6:Cr^{3+}$	52.9	885	This work
$Ca_2YSbO_6:Cr^{3+}$	23.1	945	This work
$Sr_2GaSbO_6:Cr^{3+}$	27.8	825	This work
$Sr_2InSbO_6:Cr^{3+}$	109.6	920	This work

$Sr_2YSbO_6:Cr^{3+}$	19.9	995	This work
$Ba_2ScSbO_6:Cr^{3+}$	60.3	1010	This work
$Sr_2ScSbO_6:Cr^{3+}$	149-68	895	S6
$La_2MgZrO_6:Cr^{3+}$	159-47	825	S7
$LiScP_2O_7:Cr^{3+}$	83-47	880	S8
$LaSc_3(BO_3)_4:Cr^{3+}$	130-50	871	S9
$LiInSi_2O_6:Cr^{3+}$	45-42	840	S10

The luminescence efficiency of $A_2MSbO_6:Cr^{3+}$

Figure S5 shows the quantum efficiency of $A_2MSbO_6:Cr^{3+}$ under optimal excitation. The limit of the QE instrument we used in this work is 950 nm. Therefore, the quantum efficiency of the material is calculated based on the summation of the integrated intensities of the PL spectra below 950 nm and above 950 nm. Taking $Ca_2ScSbO_6:Cr^{3+}$ and $Sr_2InSbO_6:Cr^{3+}$ as examples, the IQEs of these two samples are 71.82% and 34.7%, respectively. However, when S2 is considered, their internal quantum efficiencies are 84.3% and 64.9%, respectively.

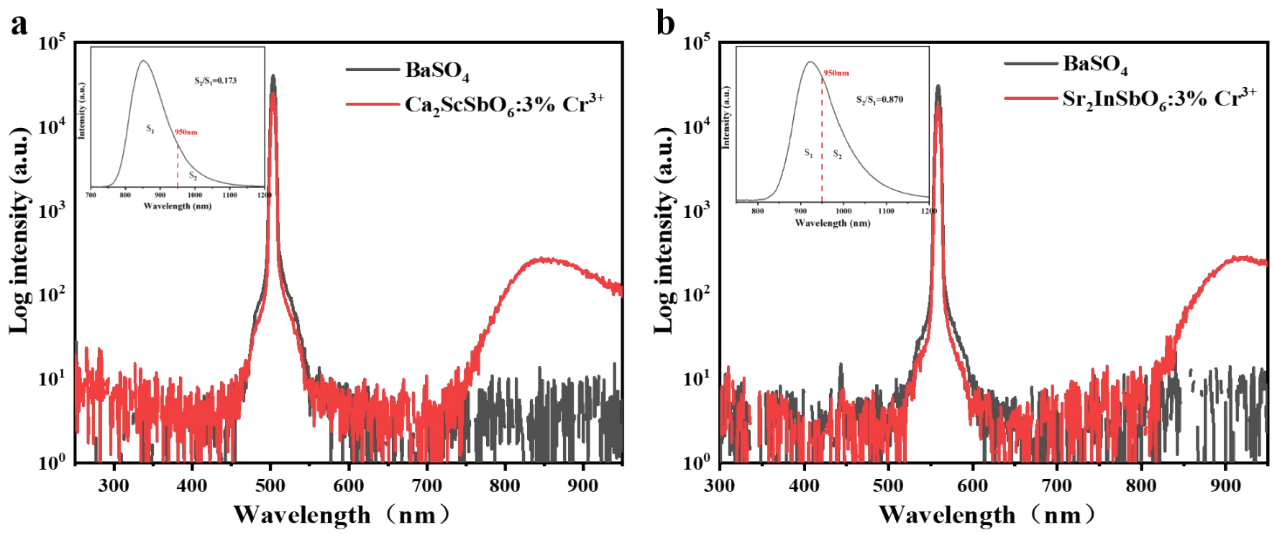

Figure S5. (a, b) PL spectra with $BaSO_4$ as the reference under the 530 and 570 nm excitation for quantum efficiency measurements of $Ca_2ScSbO_6:3\%Cr^{3+}$ and $Sr_2InSbO_6:3\%Cr^{3+}$, respectively.

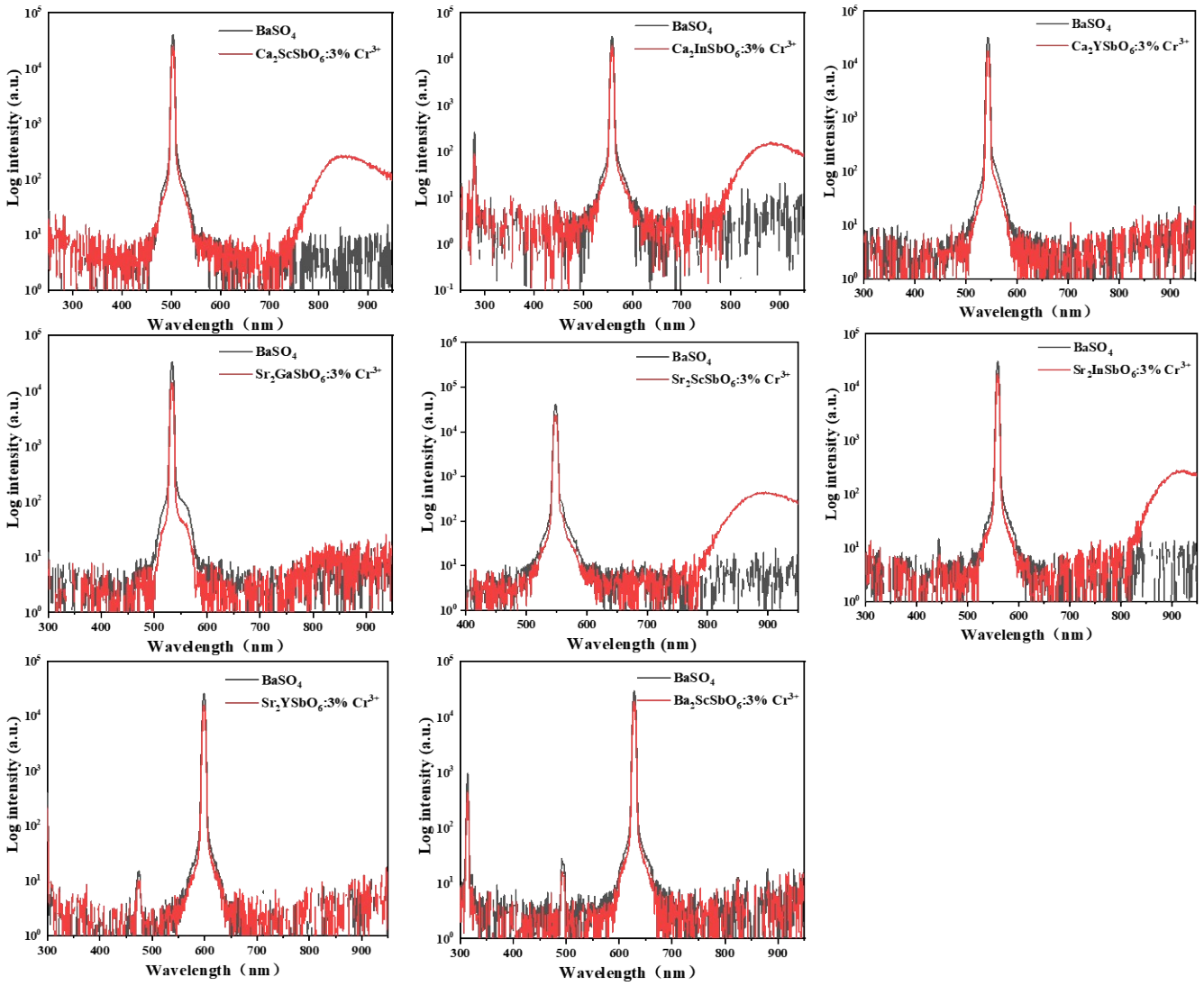

Figure S6. PL spectra with $BaSO_4$ as the reference under optimal excitation for quantum efficiency measurements of A_2MSbO_6:3% Cr^{3+}, respectively.

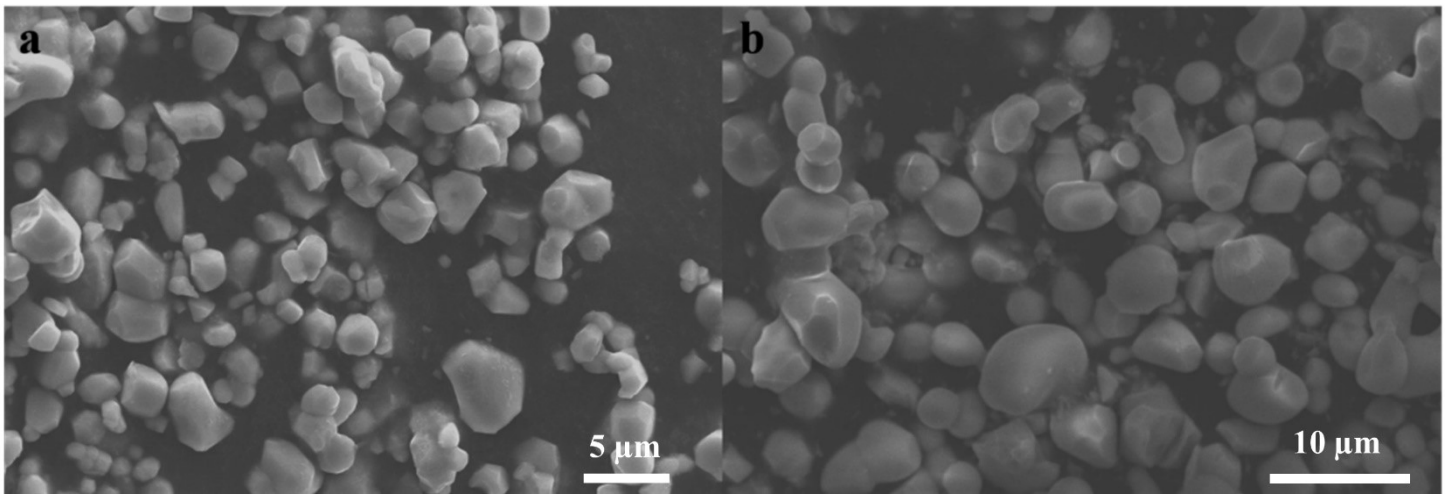

Figure S7. (a, b) SEM images of Ca_2ScSbO_6:Cr^{3+} and Sr_2InSbO_6:Cr^{3+}, respectively.

Potential Applications

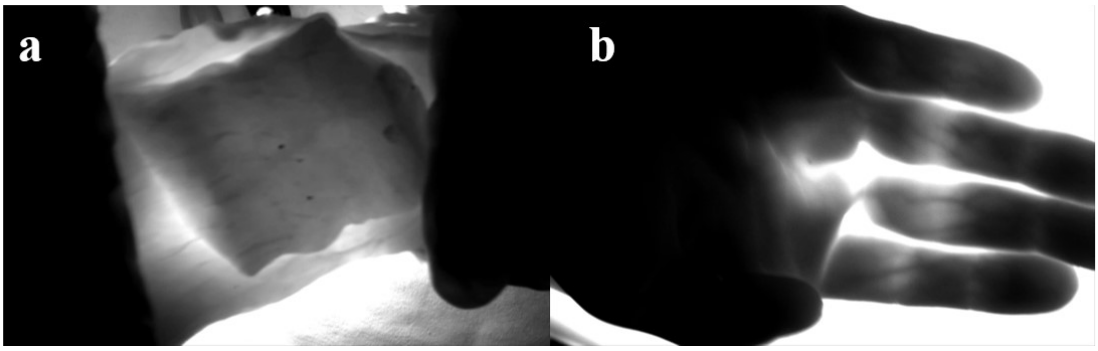

Figure S8. (a) Photograph of two layers of pork tissue and b) human fingers under $Ca_2ScSbO_6:Cr^{3+}$ based NIR pc-LED.

$Ca_2ScSbO_6:3\%Cr^{3+}$ phosphors have a characteristic NIR emission from 700 to 1100 nm, available for tissue penetration and night-vision applications. NIR pc-LEDs were fabricated by combining blue chip with both green $(Ba,Sr)_2SiO_4:Eu^{2+}$ and NIR $Ca_2ScSbO_6:Cr^{3+}$ phosphors. The thickness of a single piece of pork tissue is 1.7cm. Figure S8a is the NIR image obtained by NIR light penetrating two layers of pork tissue. It can be seen that the NIR light nearly penetrates the pork tissue. Figure S8b shows the distribution of bones and blood vessels after irradiating a human finger. This result indicates that $Ca_2ScSbO_6:Cr^{3+}$ phosphor is a promising candidate for applications in tissue penetration and medicine. The spectral tunability of bichromate allows the selection of materials with the suitable emission wavelengths for applications in complex operating environments.

References:

S1. Z. H. Sun, M. Q. Wang, Z. Yang, Z. Q. Jiang and K. P. Liu, J. Eu^{3+}-doped double perovskite-based phosphor-in-glass color converter for high-power warm w-LEDs. J. Alloys Compd., 2016, 658, 453–458.

S2. Zhou, J., Rong, X., Zhang, P., Molokeev, M. S., Wei, P., Liu, Q., Zhang, X. and Xia, Z, Manipulation of Bi3+/In3+ transmutation and Mn^{2+} doping effect on the structure and optical properties of double perovskite $Cs_2NaBi_{1-x}In_xCl_6$. Adv Opt Mater, 2019, 7, 1801435.

S3. Tanabe Y, Sugano S. On the Absorption Spectra of Complex Ions II. J. Phys. Soc. Jpn., 1954, 9: 766-779

S4. Casalboni M, Luci A, Grassano UM, et al. Optical spectroscopy of $La_3Ga_5SiO_{14}:Cr^{3+}$ crystals. Phys. Rev. B, 1994, 49 (6): 3781-3790

S5. Henderson B and Imbusch GF, Optical spectroscopy of inorganic solids, Optical spectroscopy of inorganic solids, 1989.

S6. Zhao, M.; Liu, S. Q.; Cai, H.; Zhao, F. Y.; Song, Z.; Liu, Q. L. Efficient Broadband Near-Infrared Phosphor $Sr_2ScSbO_6:Cr^{3+}$ for Solar-like Lighting. Sci. China Mater., 2021. 65, 748–756.

S7. Zeng, H. T.; Zhou, T. L.; Wang, L.; Xie, R. J. Two-Site Occupation for Exploring Ultra-Broadband near-Infrared Phosphor—Double-Perovskite $La_2MgZrO_6:Cr^{3+}$. Chem. Mater., 2019, 31 (14), 5245–5253.

S8. Yao, L. Q.; Shao, Q. Y.; Han, S. Y.; Liang, C.; He, J. H.; Jiang, J. Q. Enhancing Near-Infrared Photoluminescence Intensity and Spectral Properties in Yb^{3+} Codoped $LiScP_2O_7:Cr^{3+}$. Chem. Mater., 2020, 32 (6), 2430–2439.

S9. Gao, T. Y.; Zhuang, W. D.; Liu, R. H.; Liu, Y. H.; Yan, C. P.; Chen, X. X. Design of a Broadband NIR Phosphor for Security-Monitoring LEDs: Tunable Photoluminescence Properties and Enhanced Thermal Stability. Cryst. Growth Des., 2020, 20, 3851–3860.

S10. Liu, T.; Cai, H.; Mao, N.; Song, Z.; Liu, Q. Efficient Near-Infrared Pyroxene Phosphor LiInGe2O6: Cr3+ for NIR Spectroscopy Application. J. Am. Chem. Soc. 2021. 104 (9), 4577-4584.